WAVELET ANALYSIS OF THE SINGULAR SPECTRAL RECONSTRUCTED TIME SERIES TO STUDY THE IMPRINTS OF SOLAR-ENSO-GEOMAGNETIC ACTIVITY ON INDIAN CLIMATE

[1]S. Sri Lakshmi[*] and [2]R. K. Tiwari

[1] University Centre for Earth and Space Sciences, University of Hyderabad, Hyderabad 500 046, India
[2] CSIR-National Geophysical Research Institute, Uppal Road, Hyderabad 500 007, India

***Corresponding Author:** srilakshmi.ucess@gmail.com
Tel.: +91-40-23132671 (Office)
Fax: +91-40-23010152

ABSTRACT

To study the imprints of the Solar-ENSO-Geomagnetic activity on the Indian Subcontinent, we have applied the Singular spectral analysis (SSA) and wavelet analysis to the tree ring temperature variability record from the Western Himalayas. Other data used in the present study are the Solar Sunspot Number (SSN), Geomagnetic Indices (aa Index) and Southern Oscillation Index (SOI) for the common time period of 1876-2000. Both SSA and wavelet spectral analyses reveal the presence of 5-7 years short term ENSO variations and the 11 year solar cycle indicating the possible combined influences of solar-geomagnetic activities and ENSO on the Indian temperature. Another prominent signal corresponding to 33-year periodicity in the tree ring record suggests the Sun-temperature variability link probably induced by changes in the basic state of the earth's atmosphere. In order to complement the above findings, we performed a wavelet analysis of SSA reconstructed time series, which agrees well with our earlier results and also increases the signal to noise ratio thereby showing strong influence of solar-geomagnetic activity & ENSO throughout the entire time period. The solar flares are considered to be responsible for causing the atmospheric circulation patterns. The net effect of solar-geomagnetic processes on the temperature record might suggest counteracting influences on shorter (about 5–6 y) and longer (about 11–12 y) time scales. The present analyses suggest that the influence of solar activities on the Indian temperature variability operates in part indirectly through coupling of ENSO on multilateral time scales. The analyses, hence, provide credible evidence for tele-connections of tropical pacific climatic

variability and Indian climate ranging from inter-annual-decadal time scales and also suggest the possible role of exogenic triggering in reorganizing the global earth-ocean-atmospheric systems.

Key words: Geomagnetic activity, Western Himalayas, Sunspot Number, SOI index, Singular spectral analysis, Wavelet spectrum, Coherency.

1. Introduction:

Several recent studies of solar/geomagnetic effects on climate have been examined on both global as well as on regional scales (Lean and Rind, 2008; Benestaed and Schmidt, 2009; Meehl, 2009; Kiladis and Diaz 1989; Pant and Rupa Kumar 1997; Gray et al. 1992; Wiles et al. 1998; Friis and Svensmark 1997; Rigozo et al. 2005; Feng et al. 2003; Tiwari and srilakshmi 2009; Chowdary et al. 2006, 2014; Appenzeller et al. 1998; Proctor et al. 2002; Tsonis et al. 2005; Freitas and Mclean 2013). The Sun's long-term magnetic variability caused by the sunspots is considered as one of the primary drivers of climatic changes. The short-term magnetic variability is due to the disturbances in Earth's magnetic fields caused by the solar activities and is indicated by the geomagnetic indices. The Sun's magnetic variability modulates the magnetic and particulate fluxes in the heliosphere. This determines the interplanetary conditions and imposes significant electromagnetic forces and effects upon the planetary atmosphere. All these effects are due to the changing solar-magnetic fields, which are relevant for planetary climates including the climate of the Earth. The Sun-Earth relationship varies on different time scales ranging from days to years bringing a drastic influence on the climatic patterns. The ultimate cause of solar variability, at time scales from decadal to centennial to millennial or even longer scales has its origin in the solar dynamo mechanism. During the solar maxima, huge amounts of solar energy particles are released, thereby causing the geomagnetic disturbances. The 11 years solar cycle acts as an important driving force for variations in the space weather, ultimately giving rise to climatic changes. It is, therefore, imperative to understand the origin of space climate by analyzing the different proxies of solar magnetic variabilities. Another important phenomenon is El Nino-Southern Oscillation (ENSO), which produces droughts, floods and intense rainfall. The strong coupling and interactions between the Tropical Ocean and the atmosphere play a

major role in the development of the global climatic system. The El Nino events generally recur approximately every 3-5 years with large events spaced around 3-7 years apart. The ENSO phenomena have shown huge impact on the Asian monsoon (Cole et. al., 1993), Indian monsoon (Chowdary et al. 2006, 2014) as well as globally (Horel and Wallance 1981; Barnett 1989; Yasunari 1985; Nicholson 1997). In particular, the El Nino, solar, geomagnetic activities are the major affecting forces on the decadal and interdecadal temperature variability on global and regional scales in a direct/indirect way (El-Borie et al, 2010; Gray et al., 2010). Recent studies (Frohlich and Lean 2004; Steinhilber et al. 2009) indicate the possible influence of solar activity on Earth's temperature/climate on multi-decadal time scales. The 11 year solar cyclic variations observed from the several temperature climate records also suggest the impact of solar irradiance variability on terrestrial temperature (Budyko 1969; Friis and Lassen 1991; Friis and Svensmark 1997; Kasatkina et al. 2007). The bi-decadal (22 years) called the Hale cycle, is related to the reversal of the solar magnetic field direction (Lean et al. 1995; Kasatkina et al. 2007). The 33 year cycle (Bruckener cycle) is also caused by the solar origin, but it is a very rare cycle (Kasatkina et al. 2007). The 2–7 years ENSO cyclic pattern and its possible coupling process is the major driving force for the temperature variability (Gray et al. 1992; Wiles et al. 1998; Mokhov et al. 2000; Rigozo et al. 2007, Kothawale et al. 2010). El-Borie and Al–Thoyaib, 2006; El-Borie et al., 2007 and El-Borie et al, 2010 have indicated in their studies that the global temperature should lag the geomagnetic activity with a maximum correlation when the temperature lags by 6 years. Mendoza et. al., 1991 reported on possible connections between solar activity and El Nino's, while Reid and Gage (1988) and Reid (1991) reported on the similarities between the 11-year running means of monthly sunspot numbers and global sea surface temperature. These findings suggest that there is a possibility of strong coupling between temperature-ENSO and solar-geomagnetic signals.

The mean global temperature of the Earth's surface also plays a very important role in bringing climatic changes. Several studies have been carried out to understand the detailed climatic changes of India in the past millennium using various proxy records e.g. ice cores, lake sediments, glacier fluctuations, peat deposits etc. There is a lack of high-precision and high-resolution palaeo-climatic information for longer time scale from the Indian subcontinent. Tree-

ring data is a promising proxy to retrieve high resolution past climatic changes from several geographical regions of India (Bhattacharyya et al. 1988; Bhattacharyya et al. 1992; Hughes, 1992; Bhattacharyya and Yadav, 1996; Borgaonkar et al. 1996; Chaudhary et al. 1999; Yadav et al. 1999; Bhattacharyya and Chaudhary, 2003; Bhattacharyya et al. 2006; Shah et al. 200) It has been noted that tree-ring based climatic reconstructions in India generally do not exceed beyond 400 years records except at some sites in the Northwest Himalaya. Thus, a long record of tree-ring data is needed to extend available climate reconstruction further back to determine climatic variability on sub-decadal, decadal and century scale. However, non-availability of older living trees in most of the sites is hindering the preparation of long tree chronology. In a previous study (Tiwari and Srilakshmi, 2009), we have studied the periodicities and non-stationary modes in the tree ring temperature data from the same region (AD 1200-2000). To reveal significant connections among the Solar-geomagnetic-ENSO 'triad' phenomena on tree ring width in detail for the period from 1876-2000, we have applied here the Singular spectral analysis (SSA) and the wavelet spectral analysis for Sunspot data, geomagnetic data (aa index), Troup Southern Oscillation Index (SOI) and the Western Himalayas tree ring data. Here our main objective is to employ wavelet-based analysis on SSA reconstructed time series to find out the evidence of the possible linkages, if any, among ENSO–solar-geomagnetic in the Indian temperature records.

2. Source and Nature of Data:

The data analyzed here includes the time series of (1) Smoothed Sunspot number for solar activity (2) Geomagnetic activity data (aa indices) (3) Troup Southern Oscillation Index (SOI) for the study of El Nino-Southern Oscillation called ENSO (4) Western Himalayan temperature variability record. All the data sets have been analyzed for the common period of 125 years spanning over 1876-2000. The monthly sunspot number data has been obtained from the Sunspot Index Data Center http:// astro.oma.be/SIDC/. The Troup SOI data is obtained from the Bureau of Meteorology of Australia, http://www.bom.gov.au/climate/. The data for geomagnetic activity, aa Index, was provided by the National Geophysical Data Center, NGDC, (http://www.ngdc.noaa.gov/stp/GEOMAG/aastar.shtml). The aa index is a measure of

disturbances level of Earth's magnetic field based on magnetometer observations at two, nearly antipodal, stations in Australia and England. In recent studies, the tree ring proxy climate indicators have been potentially used for extracting information regarding past seasonal temperature or precipitation/drought based on the measurements of annual ring width. The detailed description of the data has been presented elsewhere (Yadav et. al., 2004). A brief account of the data pertinent to the present analysis, however, is summarized here. The tree ring data being analyzed here is one of the best temperature variability records (1876 to 2000) of the pre-monsoon season in the Western Himalayas available. The mean temperature series is obtained from nine weather stations including both from high and low elevation areas in the Western Himalayas. Temperature variability history is based on widely spread pure Himalayan cedar (Cedrus deodara (Roxb.) G. Don) trees and characterizes all the sites with almost no ground vegetation and thereby minimizes individual variation in tree-ring sequences induced by inter tree competition (Yadav et. al., 2004). The mean chronological structure is based on in total 60 radii from 45 trees, statistical feature of which show that the chronology is suitable for dendro-climatic studies back to AD 1226 (Yadav et. al., 2004).

3. Methods applied: To analyze the temporal series and to find the climatic structure, we have here three methods: Principal component analysis (PCA), Singular Spectral analysis (SSA) and wavelet analysis.

3.1. Principal component analysis (PCA): As a preliminary analysis, we have applied the Principle component analysis (PCA) to the data sets to extract the principle components. PCA technique is applied for the reduction and extraction for dimensionality of the data and to rate the amount of variation present in the original data set. The purpose to apply the PCA is to identify patterns in the given time series. The new components thereby obtained by the PCA analysis are termed as PC1, PC2, PC3 and so on, (for the first, second and third principal components) are uncorrelated and decrease the amount of variance from the original data set. PC1 (the first component) captures most of the variance; PC2 captures the second most of the variance and so on.

3.2. Singular spectral analysis: The Singular Spectrum Analysis (SSA) method is designed to extract as much information as possible from a short, noisy time series without any prior knowledge about the dynamics underlying the series (Broomhead and King, 1986; Vautard and Ghil, 1989; Alonso et. al., 2005; Golyandina et al., 2001). The method is a form of principal component analysis (PCA) applied to lag-correlations structures of the time series. The basic SSA decomposes an original time series into a new series which consists of trend, periodic or quasi-periodic and white noises according to the singular value decomposition (SVD) and provides the reconstructed components (RCs). The basic steps involved in SSA are: decomposition (involves embedding, singular value decomposition (SVD)) and reconstruction (involves grouping and diagonal averaging). Embedding decomposes the original time series into the trajectory matrix; SVD turns the trajectory matrix into the decomposed trajectory matrices. The reconstruction stage involves grouping to make subgroups of the decomposed trajectory matrices and diagonal averaging to reconstruct the new time series from the subgroups.

Step1: Decomposition:

(a) Embedding: The first step in the basic SSA algorithm is the embedding step where the initial time series change into the trajectory matrix. Let the time series be $Y = \{y_1, \ldots\ldots\ldots, y_N\}$ of length N without any missing values. Here the window length L is chosen such that $2 < L < N/2$ to embed the initial time series. We map the time series Y into the L lagged vectors, $Yi = \{y_i, \ldots\ldots, y_{i+L-1}\}$ for i = 1…….K, where K = N - L + 1. The trajectory matrix T_Y ($L \times K$ dimensions) is written as: $T_Y = \begin{pmatrix} Y_1 \\ Y_2 \\ . \\ . \\ Y_K \end{pmatrix}$ ……(1)

(b) Singular Value Decomposition (SVD): Here we apply SVD to the trajectory matrix T_Y to decompose and obtain $T_Y = UDV'$ called eigentriples; where U_i ($K \times L$ dimensions;$1 < i < L$) is an orthonormal matrix; D_i ($1 < i < L$) is a diagonal matrix of order L; V_i ($L \times L$ dimensions;$1 < i < L$) is a square orthonormal matrix.

The trajectory matrix is thus written as $T_Y = \sum_{i=1}^{d} U_i \sqrt{\lambda_i} V_i^T$; .....(2)

where the i[th] Eigen triple of $T_i = U_i \times \sqrt{\lambda_i} \times V_i^T$, I = 1, 2, 3..., d in which d = max(i: $\sqrt{\lambda_i} > 0$).

Step 2: Reconstruction:

(c) Grouping: Here the matrix T_i is decomposed into subgroups according to the trend, periodic or quasi-periodic components and white noises. The grouping step of the reconstruction stage corresponds to the splitting of the elementary matrices T_i into several groups and summing the matrices within each group. Let $I = \{i_1, i_2, ..., i_p\}$ be the group of indices i_1, ...i_p. Then the matrix T_I corresponding to the group I is defines as $T_I = T_{i1} + T_{i2} + ... T_{ip}$. The split of the set of indices J=1, 2, . . . ,d into the disjoint subsets $I_1, I_2, ...I_m$ corresponds to the equation (3):

$$T = T_{I1} + T_{I2} + ... T_{Im}. \quad .....(3)$$

The sets $I_1, ..., I_m$ are called the eigen triple grouping.

(d) Diagonal averaging: The diagonal averaging transfers each matrix T into a time series, which is an additive component of the initial time series Y. If z_{ij} stands for a element matrix Z, the kth term of the resulting series is obtained by averaging z_{ij} over all i, j such that i+j=k+2. This is called diagonal averaging or the Hankelization of the matrix Z. The Hankel matrix HZ, is the trajectory matrix corresponding to the series obtained by the result of diagonal averaging.

Considering equation (3), let X (L × K) matrix with elements x_{ij}, where $1 \le i \le L$, $1 \le j \le K$. Here diagonal averaging transforms matrix X to a series $g_0, ..., g_{T-1}$ using the formula:

$$g_k = \begin{cases} \dfrac{1}{k+1} \displaystyle\sum_{m=1}^{k+1} x^*_{m,k-m+2} & 0 \le k < L^* - 1 \\ \dfrac{1}{L^*} \displaystyle\sum_{m=1}^{L^*} x^*_{m,k-m+2} & L^* - 1 \le k < K^* \\ \dfrac{1}{T-k} \displaystyle\sum_{m=k-k^*+2}^{N-k+1} x^*_{m,k-m+2} & K^* - 1 \le k < T \end{cases} \quad (4)$$

This diagonal averaging by equation (4) applied to the resultant matrix X_{In}, produces time series Y_n of length T. For such signal characteristics, it is essential to examine the time-frequency

pattern as to understand whether a particular frequency is temporally consistent or inconsistent. Hence for non-stationary signals, we need a transform that will be useful to obtain the frequency content of the time series/signal as a function of time.

An alternative method for studying the non-stationarity of the time series is wavelet transform. For non-stationary signals, wavelets decomposition would be the most appropriate method because the analyzing functions (the wavelets function) are localized both in time and frequency.

3.3. Wavelet spectral analysis: During the past decades, wavelet analysis has become a popular method for the analysis of aperiodic and quasi-periodic data (Grinsted et. al., 2004; Jevrejeva et. al., 2003; Torrence and Compo, 1998; Torrence and Webster, 1999). In particular, it has become an important tool for studying localized variations of power within a time series. By decomposing a time series into time-frequency space, the dominant modes of variability and their variation with respect to time can be identified. The wavelet transform has various applications in geophysics, including tropical convection (Weng and Lau 1994), the El Niño–Southern Oscillation (Gu and Philander 1995), etc. We have applied the wavelet analysis to analyze the non-stationary signals which permits the identification of main periodicities of ENSO-sunspot-geomagnetic in the time series. The results give us more insight information about the evolution of these variables in frequency-time mode.

A wavelet transform requires the choice of analyzing function Ψ (called "mother wavelet") that has the specific property of time-frequency localization. The continuous wavelet transform revolves around decomposing the time series into scaling components for identifying oscillations occurring at fast (time) scale and other at slow scales. Mathematically, the continuous wavelets transform of a time series f(t) can be given as:

$$W_{\psi}(f)(a,b) = \frac{1}{\sqrt{a}} \int_{-\infty}^{\infty} f(t)\psi\left(\frac{t-b}{a}\right)dt \quad \text{.....(5)}$$

Here f(t) represents time series, Ψ is the base wavelets function (here we have chosen the Morlet function), with length that is much shorter than the time series f(t). W stands for wavelet coefficients. The variable 'a' is called the scaling parameter that determines the

frequency (or scale) so that varying 'a' gives rise to wavelet spectrum. The factor 'b' is related to the shift of the analysis window in time so that varying b represents the sliding method of the wavelet over f(t).

In several recent analyses, complex Morlet wavelet has been found useful for geophysical time series analysis. The Morlet is mostly used to find out areas where there is high amplitude at certain frequencies. The complex Morlet wavelet can be represented by a periodic sinusoidal function with a Gaussian envelope and is excellent for Morlet wavelet may be defined mathematically, as follows:

$$\psi(t) = \pi^{-1/4} e^{-i\omega_0 t} e^{-t^2/2} \quad \text{.....(6)}$$

where ω_0 is a non-dimensional value. ω_0 is chosen to be 5 to make the highest and lowest values of ψ approximately equal to 0.5, thus making the admissibility condition satisfied. The complex valued Morlet transform enables to extract information about the amplitude and phase of the signal to be analyzed. Wavelet transform preserves the self-similarity scaling property, which is the inherent characteristic feature of deterministic chaos. The continuous wavelet transform has edge artifacts because the wavelet is completely localized in time. The cone of influence (COI) is the area in which the wavelet power caused by a discontinuity at the edge has dropped to e^{-2} of the value to the edge. The statistical significance of the wavelet power can be assessed relative to the null hypotheses that the signal is generated by a stationary process with a given background power spectrum (P_k) of first order autoregressive (AR1) process. (Grinsted et. al., 2004)

$$P_k = \frac{1-\alpha^2}{\left|1-\alpha e^{-2i\pi k}\right|^2} \quad \text{.....(7)}$$

where k is Fourier frequency index.

The cross wavelet transform is applied to two time series to identify the similar patterns which are difficult to assess from a continuous wavelet map. Cross wavelet power reveals areas with high common power. The cross wavelet of two time series x (t) and y (t) is defined as W^{XY} =

$W^X W^{Y*}$, where * denotes complex conjugate. The cross wavelet power of two time series with background power spectra P_k^X and P_k^Y is given as

$$D\left(\frac{\left|W_n^X(s)W_n^{Y*}(s)\right|}{\sigma X \sigma Y} < p\right) = \frac{Z_v(p)}{v}\sqrt{P_k^X P_k^Y}, \quad \text{.....(8)}$$

where $Z_v(p)$ is the confidence level associated with the probability p for a pdf defined by the square root of the product of the two χ^2 distributions (Torrence and Compo, 1998). The wavelet power is $\left|W_n^X(s)\right|^2$ and the complex argument of $\left|W_n^X(s)\right|$ can be interpreted as the local phase. The cross wavelet analysis gives the correlation between the two time series as function of period of the signal and its time evolution with a 95% confidence level contour. The statistical significance is estimated using red noise model.

Wavelet coherence is another important measure to assess how coherent the cross wavelet spectrum transform is in time frequency space. The wavelet coherence of two time series is defined as (Torrence and Webster, 1998)

$$R_n^2(s) = \frac{\left|S(s^{-1}W_n^{XY}(s))\right|^2}{S(s^{-1}\left|W_n^X(s)\right|^2).S(s^{-1}\left|W_n^Y(s)\right|^2)} \text{.....(9)}$$

where S is a smoothing operator. The smoothing operator is written as S (W) = $S_{scale}(S_{time}(W_n(s)))$, where S_{scale} denotes smoothing along the wavelet scale axis and S_{time} smoothing in time. Here for the morelet wavelet, the smoothing operator is

$$S_{time}(W)\big|_s = \left(W_n(s) * c_1^{\frac{-t^2}{2s^2}}\right) \text{.....(10)}$$

$$S_{time}(W)\big|_s = \left(W_n(s) * c_2\Pi(0.6s)\right)_n\big| \text{.....(11)}$$

Where c_1 and c_2 are normalization constants and Π is the rectangle function. The factor of 0.6 is empirically determined scale decorrelation length of the Morlet wavelet (Torrence and Compo, 1998). The statistical significance level of the wavelet coherence is estimated using the Monte Carlo methods (Grinsted et. al., 2004).

4. Results and Discussion:

We analyzed the data sets spanning over the period of 1876-2000 using the PCA, SSA and wavelet spectral analyses. Figure 1 shows four time series: (1) Smoothed Sunspot number representing solar activities; (2) Geomagnetic (aa indices); (3) Troup Southern Oscillation Index (SOI) for the study of ENSO and (4) Western Himalayan temperature variability record that are analyzed in the present work. From visual inspection it is apparent from Fig. 1 that both WH and SOI data show irregular and random pattern, while sunspot numbers have quasi- cyclic character. Further WH tree ring record also exhibits distinct temperature variability but nonstationary behavior at different scales. This variability might be suggestive of coupled global ocean-atmospheric dynamics or some other factors, such as deforestation, anthropogenic, high latitudinal influence etc (Yadav et. al., 2004).

(Figure 1)

Hence it is quite difficult to differentiate such a complex climate signals visually and difficult to infer any clear oscillation without the help of powerful mathematical methods. For identification of any oscillatory components and understanding the climatic variations on regional and global scale, we have applied the PCA, SSA and wavelet analysis. Figure 2 shows the principal components (PCs) for the first four eigen triples (PC1, PC2, PC3, PC4) for the given data sets. Figure 3 shows the power spectra of the principal components (PCs) for the four data sets shown in figure 2. From the figure 3, it is observed that the power spectra of PC1-4 for the sunspot data exhibits high power at 124, 11, 4-2.8 years. The presence of high solar signal at 124 years indicates the quasi-stable oscillatory components in the data. The power spectra of geomagnetic data also shows the presence of strong signals at 124, 10-11, 4-2 years suggesting a strong link of solar-geomagnetic activity. The power spectra of WH temperature data shows strong high power at ~62 years, 32-35 years, 11 years, 5 years and 2-3 years suggesting a strong influence of solar-geomagnetic-ENSO effects on the Indian climate system. Dominant amplitude is found at 32-35 years corresponding to Atlantic Multi-decadal Oscillation (AMO) cycles. These results can be better confirmed by applying the mathematical tools of SSA and wavelet analysis.

(Figure 2 & 3)

To explore the stationary characteristics of these peaks obtained by the PCA, we have applied the Morlet based wavelet transform approach (Holschneider, 1995; Foufoula-Georgiou and Kumar, 1995; Torrence and Compo, 1998; Grinsted et. al., 2004). The wavelet spectrum identifies the main periodicities in the time series and helps to analyze the periodicties with respect to time. Figure 4 shows the wavelet spectrum for the a) Smoothed Sunspot number for solar activity (SSN) (b) Western Himalayan (WH) temperature variability record (c) Geomagnetic activity and (c) Troup Southern Oscillation Index (SOI). From the wavelet spectrum of sunspot time series (Figure 4a), the signal near 11-year is the strongest feature and is persistent during the entire series indicating the non-stationary behavior of the sunspot time series. The wavelet spectrum of SOI (figure 4c) shows strong amplitudes. However, due to non-stationary (time variant) character of the time series, the observed spectral peaks (power) split in the interval of 2- 8 years. The wavelet power spectrum of the western Himalayan temperature variability (Figure 4b) reveals significant power concentration at inter-annual time scales of 3-5 years and at 11 years solar cycle. A dominant amplitude modes is also seen in the low frequency range at around 35-40 years (at periods 1930-1980) corresponding to AMO cycles. Our result agrees well with the results of other climate reconstructions (Mann et. al., 1995) from tree rings and other proxies. The observed variability in AMO periodicity has also been reported in other tree ring record (Gray et. al., 2004). The statistical significance of the wavelet power spectrum is tested by a Monte Carlo method (Torrence and Compo, 1998). The WH spectra depicting statistically significant powers at around 5 years, 11 years and 33 years above the 95% significance level, suggests a clear picture of the imprint of sunspot-geomagnetic and ENSO on the tree ring data. The wavelet power spectrum of the geomagnetic record (Fig. 4d) indicates significant power on shorter scales around 2, 4-8, 11 years period.

(Figure 4)

In order to have better visualization of similar periods in two time series and for the interpretation of the results, cross wavelet spectrum has been applied. Figure 5 shows the cross wavelet spectrum of the a) SSN-WH temperature data b) WH data-SOI and c) SSN-SOI data. The contours (dark black lines) are the enclosing regions where wavelet cross power is significantly

higher, at 95% confidence levels. The wavelet cross-spectra of WH-SSN (Fig.5a) show statistically significant high power over a period of 1895-1985 in 8-16 years band. It is seen that the WH-SOI cross-spectra (Fig. 5b), the high power is observed at 2–4 year band and 8–16 years as well. The SSN-SOI spectra (Fig. 5c) shows a strong correlation at 11 years solar cycle, which is stronger during 1910-1950 and 1960-2000 (Rigozo et. al., 2002, Rigozo et. al., 2003) suggesting the strongest El Nino and La Nina events indicating solar modulation on ENSO (Kodera, 2005; Kryjov and Park, 2007). These results show a good correspondence in response of growth of the tree ring time series during the intense solar activity. Hence the results strongly support the possible origin of these periodicities from Solar and ENSO events. The interesting conclusion from Fig. 5 is that WH–sunspot connections are strong at 11 years, ENSO–sunspot also exhibit strong power around 11 years; the WH–ENSO connections are spread over three bands, the 2–4 y; 4–8 and 8–16 y, covering the solar cycle and its harmonics; the WH-geomagnetic exhibits strong connections around 2-4, 4-6, 11 years and 35-40 years indicating the influence of solar-geomagnetic activity on Indian temperature.

(Figure 5)

The Singular spectral analysis (SSA) is performed for all the four data sets with window length of 40. The SSA spectra with 40 singular values and its corresponding reconstructed series (varying from RC1-15 in some cases) are plotted are shown in Figure 6 &7. The important insights from SSA spectra are the identification of gaps in the eigen value spectra. As a rule, the pure noise series produces a slowly decreasing sequence of singular values. The explicit plateau in the spectra represents the ordinal numbers of paired eigen triples. The eigen triples 2-3 for the sunspot data corresponds to 11 years period; eigen triples for 1-2,3-5,6-10,11-14 for the WH temperature data are related to harmonic with specific periods (periods 33-35, 11, 5, 2); eigen triples for 2-5,6-9,10-13 for the geomagnetic data are related to periods 11, 5,2 years. The eigen triples for the SOI data represents to ~ 5-7, 2 years periods. In order to assess periodicities, the periodogram and the wavelet power spectra are plotted using the SSA reconstructed data (SSA-RC) (Figure 8). From the figure 8, the periodogram of SSA-RC of SSN and Geomagnetic data shows strong power at ~120, 10-11 years; the SOI data shows strong

359 peaks at 6-9, 3, years & WH data shows strong power at ~32, ~10-11, 3-5 years. The wavelet
360 spectra for all the SSA-RC data confirms the results excepts for periods at ~120 years as the
361 scaling period for the wavelet spectra is 64 years period. The coherency plot of the SSA-RC data
362 sets (Figure 9) indicates a significant power at 33 years, 11 years, 2-7 years in the WH
363 temperature record suggesting the possible influences of Sunspot-geomagnetic activity and
364 ENSO through tele-connection and hence significant role of these remote internal oscillations of
365 the atmosphere-ocean system on the Indian climate system. Researchers have attributed these
366 phenomena to internal ocean dynamics and involve ocean atmospheric coupling as well as
367 variability in the strength of thermohaline circulations (Knight et. al., 2005; Delworth and Mann,
368 2000).

369 **(Figures 6, 7, 8 & 9)**

370 In general our result agrees well with earlier findings in the sense that statistically
371 significant global cycles of coupled effects of Sunspot/geomagnetic and ENSO are present in the
372 land based temperature variability record. However, there are certain striking features in the
373 spectra that need to be emphasized regarding the western Himalayas temperature variability: i)
374 Inter-annual cycles in period range of 3-8 years corresponding to ENSO in the wavelet spectra
375 exhibit intermittent oscillatory characteristics throughout the large portion of the record (Fig 4);
376 ii) The 11 years solar cycle in the cross wavelet spectrum of SSN and SOI (Figure 5) indicate the
377 solar modulation in the ENSO phenomena (Kodera, 2005; Kryjov and Park, 2007). iii) The high
378 amplitude at 11 years in the time intervals 1900-1995 with a strong intensity from 1900-1995
379 shows a good correspondence with the high temperature variability for the interval of high
380 solar-geomagnetic activity. The Multi-decadal (30-40 years) periodicity identified here in
381 Western Himalayan tree ring temperature record matches with North Atlantic sea surface
382 temperature variability implying that the temperature variability in the western Himalayan is
383 not a regional phenomenon, but a globally tele-connected climate phenomena associated with
384 the global ocean-atmospheric dynamics system (Tiwari & srilakshmi, 2009; Delworth et. al.,
385 1993; Stocker, 1994). The coupled ocean-atmosphere system appears to transport energy from
386 the hot equatorial regions towards Himalayan territory in a cyclic manner. These results may
387 provide constraints for modeling of climatic variability over the Indian region and ENSO

phenomena associated with the redistribution of temperature variability. The solar-geomagnetic effects play a major role in abnormal heating of the land surface thereby indirectly affects the atmospheric temperature gradient between the land-ocean coupled systems. In the present work, the connections between solar/geomagnetic activity and ENSO on the WH time series are found to be statistically significant, especially when they are studied over contrasting epochs of respectively high and low solar activity. The correlation plots for the SSA-RC data sets of WH-sunspot, WH-aa index, WH-SOI and Sunspot-aa index are plotted in figure 10. It is noticed that there is a correlation plots for the Geomagnetic-sunspot activity has a maximum correlation value at 1 year lag suggesting the strong influence of sunspot & geomagnetic forcing on one another. The cross-correlation plot for the WH data and the SOI represents a maximum value at zero lag. The correlations plot for WH-sunspot & WH-geomagnetic index exhibits almost the identical results suggesting the possible impact of solar activities on the Indian temperature variability.

(Figures 10)

The net effect of solar activity on temperature record therefore appears to be the result of cooperating or counteracting influences of earth's magnetic activity on the shorter and longer periods, depending on the indices used; scale-interactions, therefore, appear to be important. Nevertheless, the link between Indian climate and solar/geomagnetic activity emerges as having the strong evidence; next is the ENSO–solar activity connection.

5. Conclusions:

In the present paper, we have studied and identified the periodic patterns from the published Indian temperature variability records using the modern spectral methods of Singular spectral analysis (SSA)-Wavelet methods. The application of wavelet analysis for the SSA reconstructed time series, along with the removal of noise in the data identifies the existence of a high-amplitude, recurrent, multi-decadal scale patterns that are present in Indian temperature records. The power spectra of WH temperature data shows strong high power at ~62 years, 32-35 years, 11 years, 5 years and 2-3 years suggesting a strong influence of solar-geomagnetic-ENSO effects on the Indian climate system. The presence of dominant amplitude at 33-year

cycle periodicity corresponds to Atlantic Multidecadal Oscillation (AMO) cycles. It also suggests the Sun-temperature variability probably involving the induced changes in the basic state of the atmosphere. The 30-40 yrs periodicity in Western Himalayan tree ring temperature record matches with the global signal of the coupled ocean-atmospheric oscillation (Delworth et. al., 1993; Stocker, 1994) implying that the temperature variability in Himalayan is not a regional phenomenon, but seems to be tele-connected phenomena with the global ocean-atmospheric climate system. The coherency plots of the SSA reconstructed WH-Sunspot; WH-geomagnetic and WH-SOI data sets show strong spectral signatures in the whole record confirming the possible influences of Sunspot-geomagnetic activities and ENSO through teleconnection and hence the significant role of these remote internal oscillations of the atmosphere-ocean system on the Indian temperatures. We conclude that the signature of solar-geomagnetic activity affects the surface air temperatures of Indian subcontinent. However, long data sets from the different sites on the Indian continent are necessary to identify the influences of the 120 years solar-geomagnetic cycles.

Acknowledgements

The authors are extremely thankful to the anonymous reviewers for their professional comments, meticulous reading of the manuscript and valuable suggestions to improve the manuscript. The authors thank Dr. Ram Ratan Yadav, Birbal Sahni Institute of Palaeobotany, India for providing the Western Himalayan data. The authors acknowledge Dr. Francisco Javier Alonso of University of Extremadura for using the SSA routine in a MATLAB environment. We are thankful to Dr. Grinsted and his colleagues for providing the wavelet software package. First author acknowledged the Head, University Centre for Earth & Space Sciences, University of Hyderabad for providing the facilities to carry out this work. RKT is grateful to DAE for RRF.

References

Alonso, F. J., Castillo, J., and Pintado, P. (2005), "Application of Singular Spectrum Analysisto the Smoothing of Raw Kinematic Signals," Journal of Biomechanics, 38(5), 1085–1092.

445 Appenzeller, C., Stocker, T. F., and Anklin, M. (1998). North Atlantic Oscillation Dynamics Record in
446 Greenland Ice Cores. Science, 282(5388), 446–449.
447 Barnett, T.P., et al. (1989). The effect of Eurasian snow cover on regional and global climate
448 variations. J. Atmos. Sci., 48, 661–685.
449 Benestaed, R.E., and Schmidt, G.A., (2009), Solar trends and global warming, Journal of Geophysical
450 research, P 114.
451 Bhatacharyya A, LaMarche VC, and Telewski FW, (1988) Dendrochronological reconnaissance of the
452 conifers of Northwest India, Tree-Ring Bull., 48: 21-30.
453 Bhattacharyya A, and Chaudhary V, (2003) Late-summer temperature reconstruction of the Eastern
454 Himalayan Region based on tree-ring data of Abies densa, Arct. Antarct. Alp.Res., 35(2): 196-202.
455 Bhattacharyya A, and Yadav RR, (1996) Dendrochronological reconnaissance of Pinus wallichiana to
456 study glacial behaviour in the western Himalaya. Current Science, 70 (8): 739-744.
457 Bhattacharyya A, Shah, Santosh K, and Chaudhary V, (2006) Would tree-ring data of Betula utilis be
458 potential for the analysis of Himalayan Glacial fluctuations?, Current Science, 91(6): 754-761.
459 Bhattacharyya A, Yadav RR, Borgaonkar HP, & Pant GB, (1992) Growth ring analysis of Indian tropical
460 trees: Dendroclimatic potential, Current Science, 62: 736-741.
461 Bhattacharyya, A. and Yadav, R.R., (1992) Tree growth and recent climatic changes in the western
462 Himalaya, GeophytoJogy, 22, 255-260.
463 Bigg GR, (1996) The oceans and Climate, Cambridge University Press, Cambridge, 1-266.
464 Borgaonkar HP, Pant GB, & Rupa Kumar k, (1996) Ring width variations in Cedrus deodara and its
465 climatic response over the Western Himalaya. Intern. J. Climatol. 16: 1409-1422.
466 Broomhead, D.S., and King, G.P., (1986). Extracting qualitative dynamics from experimental data,
467 Physica D 20, 217–236.
468 Budyko, M. I. (1969). The effect of solar radiation variations on the climate of the Earth. Tellus, 21,
469 611–619
470 Cane MA, (1992) Tropical Pacific ENSO models: ENSO as a mode of the coupled system. In: Climate
471 System Modelling, Ed: K.E. Trenberth, Cambridge University Press, Cambridge, 583-614.
472 Chaudhary V, Bhattacharyya A, and Yadav RR, (1999) Tree-ring studies in the Eastern Himalayan
473 region: Prospects and problems, IAWA, .20(3): 317-324.

474 Chowdary, J. S., John, N., and Gnanseelan, C. (2014). Interannual variability of surface air-
475 temperature over India: impact of ENSO and Indian Ocean Sea surface temperature. Int. J.
476 Climatol., 34, 416–429.
477 Chowdary, J.S., Gnanseelan, C., Vaid, B.H., and Salvekar, P.S. (2006). Changing trends in the tropical
478 Indian Ocean SST during La Nina years. Geophys. Res. Lett., 33, L18610. doi:10.1029/
479 2006GL026707.
480 Cole JE, Fairbanks RG, and Shen GT, (1993) Recent variability in the Southern Oscillation: Isotopic
481 results from a Tarawa Atoll coral. Science, 260: 1790-1793.
482 De Freitas, C., and Mclean, J. (2013). Update of the Chronology of Natural Signals in the Near Surface
483 Mean Global Temperature Record and the Southern Oscillation Index. International Journal of
484 Geosciences, 4 (1), 234–239.
485 Delworth T, and Mann M, (2000) Observed and Stimulated multideacadl variability in the Northern
486 Hemisphere, 16: 661-676.
487 Delworth T, Manabe S & Stouffer RJ (1993) Interdecadal variations of the thermohaline circulation in
488 a coupled ocean-atmosphere model. J. Climate 6: 1991-2011.
489 El–Borie, M.A., Shafik, E., Abdel–Halim, A.A., El–Monier, S., (2010), Spectral analysis of solar
490 variability and their possible role on the global warming (1880-2008), Journal of Enviromental
491 Protection, 1, pp 111-120.
492 El–Borie, M.A., Al. Thoyaib, S.S, Al–Sayed, N., (2007), The 2nd Inter. CPMS, 302.
493 El-Borie, M.A., and Al-Thoyaib, S.S., (2006), Can we use the aa geomagnetic activity index to predict
494 partially the variability in global mean temperature, Journal of Physical Sci.,1(2), pp 67–74.
495 Feng, S.H., Kaufman, D., Yoneji, S., Nelson, D., Shemesh, A., Huang, Y., Tian, J., Bond, G., Benjamin, C.,
496 and Brown, T. (2003). Cyclic Variation and Solar Forcing of Holocene Climate in the Alaskan
497 Subarctic. Science, 301, 1890–1893.
498 Foufoula-Georgiou E, and Kumar P, (Eds.), (1995) Wavelets in Geophysics, Academic San Diego, Calif.,
499 373pp.
500 Friis, C.E., and Lassen, K. (1991). Length of the Solar Cycle: An Indicator of Solar Activity Closely
501 Associated with Climate. Science, 254 (5032), 698–700.

Friis, C.E., and Svensmark, H. (1997). What do we really know about the sun- climate connection?, Adv. Space Res., 20, 415, 913–9211.

Frohlich, C., and Lean, J. (2004). Solar radiative output and its Variability: Evidence and Mechanisms. The Astron Astropys Rev., 12, 273–320.

Golyandina, N., Nekrutkin, V. V., and Zhigljavski, A. A. (2001), Analysis of Time Series Structure: SSA and Related Techniques, Boca Raton: CRC Press.

Gray L.J.,Beer, J., Geller, M., Haigh,J.D., Lockwood, M., Matthes, K., Cubasch, U., Fleitmann,D., Harrison,G., Hood,L., Luterbacher,J., Meehl,G.A., Shindell, D.,vanGeel B., and White, W., (2010). Solar influences on climate, Reviews of Geophysics, 48, RG 4001, doi: 10.1029/2009RG000282.

Gray ST, Graumlich LJ, Betancourt JL, and Pederson GT, (2004) A tree-ring based reconstruction of the Atlantic Multidecadal Oscillation since 1567 A.D, Geophys. Res. Lett. , 31: L12205, doi:10.1029/2004GL019932.

Gray, W. M., Sheaffer, J. D., and Knaff, J. A. (1992). Hypothesized mechanism for stratospheric QBO influence on ENSO variability. Geophy. Res. Let., 19, 107–110.

Grinsted A, Moore JC, Jevrejeva S (2004) Application of the cross wavelet transform and wavelet coherence to geophysical time series, Nonlin. Processes Geophys., 11: 561–566, doi:10.5194/npg-11-561-2004

Gu, D., and Philander, S.G.H., (1995). Secular changes of annual and inter-annual variability in the tropics during the past century, J. Clim. 8, 64–876.

Holschneider M (1995) Wavelets: An Analysis Tool, Oxford University Press, New York, 455.

Horel, J.D., and Wallance, J.M.(1981). Planetary-scale atmospheric Phenomena associated with the Southern Oscillation, Monthly weather review, 109, 813-829.

Hughes MK (1992) Dendroclimatic evidence from the Western Himalaya. In: R.S. Bradlay & D.Jones(eds.),ClimatesinceAD 1500:4 15-431.Routledge.London.

Jevrejeva S, Moore JC, Grinsted A (2003) Influence of the Arctic Oscillation and El Niño-Southern Oscillation (ENSO) on ice conditions in the Baltic Sea: The wavelet approach, J. Geophys. Res., 108(D21), 4677, doi:10.1029/2003JD003417.

529 Ji JF, Shen J, Balsam W, Chen J, Liu L & Liu XQ, (2005) Asian monsoon oscillations in the northeastern
530 Qinghai-Tibet Plateau since the late glacial as interpreted from visible reflectance of Qinghai Lake
531 sediments, Earth and Planetary Science letters 233: 61-70.
532 Kasatkina, E.A., Shumilov, O.I., and Krapiec, M.(2007). On periodicities in long term climatic variations
533 near 68_N, 30_E. Adv. Geosci, 13, 25–29.
534 Kiladis, G.N., and Diaz, F.H. (1989). Global Climatic Anomalies Associated with Extremes in the
535 Southern Oscillation. J. Climate, 2, 1069–1090.
536 Knight JR, Allan RJ, Folland CK, Vellinga M, and Mann ME, (2005) A signature of persistent natural
537 thermohaline circulation cycles in observed climate'. Geophys. Res. Lett., 32, L20708,
538 doi:10.1029/2005GL024233.
539 Kodera, K., and Y.Kuroda (2005). A possible mechanism of the spatial structure of the North Atlantic
540 Oscillation, Journal of Geophysics Research, 110, D02111, doi: 10.1029/2004JD005258.
541 Kothwale, D.R., Munot, A.A., and Krishna Kumar, K. (2010). Surface air temperature variability over
542 India during 1901-2007 and its association with ENSO. Climate Research, 42, 89–104,
543 doi:10.3354/cr00857.
544 Kryjov, V.N., and Park, Chung-Kyu, (2007). Solar modulation of the El-Nino/Southern Oscillation
545 impact on the Northern Hemisphere annular mode, Geophysical research letters, Vol. 34,
546 L10701, doi: 10.1029/2006GL028015.
547 Lean, J.L. and Rind, D.H., (2008), How natural and anthropogenic influences alter global and
548 regional surface temperatures: 1889 to 2006, Journal of Geophysical Research, Letter, p 35.
549 Lean, J., Beer, J., and Bradley, R. (1995). Reconstruction of solar irradiance since 1610: Implications
550 for climate change. Geophy. Res.Lett., 22, 3195-3198.
551 Mann ME, Park J, and Bradley RS, (1995) Global interdecdal and century-scale climate oscillations
552 during the past 5 centuries, Nature, 378: 266–27.
553 Meehl, G.A., Arblaster, J.M., Matthes, K., Sassi, F., and Van Loon, H. (2009). Amplifying the Pacific
554 climate system response to a small 11-year solar cycle forcing. Science, 325, 1114–1118.
555 Mendoza B, Perez-Enriquez R, and Alvarez-Madrigal M, (1991) Analysis of solar activity conditions
556 during periods of El Nino events, Ann. Geophysicae, 9: 50-54.

557 Mokhov, I. I., Eliseev, A.V., Handorf, D., Petukhov, V.K., Dethloff, K., Weishiemer, A., and
558 Khvorostyanov, D. V. (2000). North Atlantic Oscillation: Diagnosis and simulation of decadal
559 variability and its long period evolution. Atmospheric and Ocean physics, 36, 555–565.
560 Nicolson, S. E. (1997). An analysis of the Enso signal in the tropical Atlantic and western Indian
561 oceans. Int. J. Climatol., 17, 345–375.
562 Pant, G.B., and Rupa Kumar, K. (1997). Climates of South Asia. John Wiley and Sons, Chichester, 320
563 pp.
564 Philander SG, (1990) El Nino, La Nina and the Southern Oscillation. Academic Press, London, 1-293.
565 Proctor, C.J., Baker, A., and Barnes, W. L. (2002). A three thousand year record of North Atlantic
566 Climate. Clim.Dyn, 19, 449–454.
567 Reid GC and Gage KS, (1988) The climatic impact of secular variations in solar irradiance, in Secular
568 Solar and geomagnetic Variations in the Last 10000 years', Eds. F.R. and A.W. Wplfendale, NATO
569 AS Series, Kluwer, Dordrecht, 225-243.
570 Reid GC, (1991) Solar irradiance variations and global Ocean Temperature, Journal of Geomagn.
571 Geoelectr., 43: 795-801.
572 Rigozo NR, Noredmann DJR, Echer E, Zanandrea A, Gonzalez WD, (2002) Solar variability effects
573 studied by tree-ring data wavelet analysis, Adv. Space Res., 29(12): 1985-1988.
574 Rigozo NR, Vieira Lea, Echer E, Nordemann DJR, (2003) Wavelet analysis of Solar-ENSO imprints in
575 tree-ring data from Southern Brazil in the last century, Climatic change, 60: 329-340.
576 Rigozo, N. R., Nordeman, D. J. R., Echer, E., Vieira, L. E. A., Echer M. P. S. and Presets, A.(2005). Tree-
577 ring width wavelet and spectral analysis of solar variability and climatic effects on a Chilean
578 cypress during the last two and a half millennia. Climate of the Past Discussions, 1, 121–135.
579 Rigozo, N. R., Nordeman, D.J.R., Silva, H.E., Echer, M.P.S. and Echer, E. (2007). Solar and climate signal
580 records in tree ring width from Chile (AD1587–1994). Planetary and Space Science, 55, 158–164.
581 Shah Santosh K, Bhattacharyya A, and Chaudhary V, (2007) Reconstruction of June-September
582 Precipitation based on tree-ring data of Teak (Tectona grandis L.) from Hoshangabad, Madhya
583 Pradesh, India. Dendrochronologia, 25: 57-64.
584 Steinhilber, F., Beer, J. and Frohlich, C. (2009). Total solar irradiance during the Holocene. Geophys.
585 Res. Lett., 36, L19704.

586 Stocker TF (1994). The variable ocean. Nature 367: 221-222.
587 Tiwari RK, and Srilakshmi S, (2009). Periodicities and non-stationary modes in tree ring temperature
588 variability record of the Western Himlayas by multitaper and wavelet spectral analyses, Current
589 Science, 97, 5: 705-709.
590 Torrence C, Compo GP, (1998). A practical guide to wavelet analysis, Bull. Am. Meteorol. Soc., 79: 61–
591 78
592 Torrence C, Webster P, (1999). Interdecadal changes in the ESNO-Monsoon System, J.Clim., 12:
593 2679–2690.
594 Trenberth K, and Hoar TJ, (1997). El Nino and climate change. Geophys. Res. Lett., 24: 3057–3060.
595 Tsonis, A. A., Elsner, J. B., Hunt, A. G., and Jagger, T. H. (2005). Unfolding the relation between global
596 temperature and ENSO. Geophy.Res.Lett.,32, L09701.
597 Vautard, R., and Ghil, M. (1989). Singular spectrum analysis in nonlinear dynamics, with applications
598 to paleoclimatic time series. Phys. D, 35, 395–424.
599 Weng, H., and K.-M. Lau, 1994: Wavelets, period doubling, and time-frequency localization with
600 application to organizationmof convection over the tropical western Pacific. J. Atmos. Sci., 51,
601 2523–2541.
602 Wiles, G. C., D'Arrigo, R. D., and Jacoby, G. C. (1998). Gulf of Alaska atmosphere-ocean variability over
603 recent centuries inferred from coastal tree-ring records, Climatic Change, 38,
604 Yadav RR, Park WK, and Bhattacharyya A, (1999) Spring-temperature variations in western Himalaya,
605 India, as reconstructed from tree-rings: AD 1390-1987, The Holocene, 9(1): 85-90.
606 Yadav RR, Park WK, Singh J & Dubey B, (2004) Do the western Himalayas defy global warming?',
607 Geophysical Research Letters 31: L17201, doi: 10.1029/2004GL020201.
608 Yasunari, T. (1985). Zonally propagating modes of the global east–west circulation associated with
609 the Southern Oscillation. J. Meteorol. Soc. J., 63, 1013–1029.
610
611
612
613
614

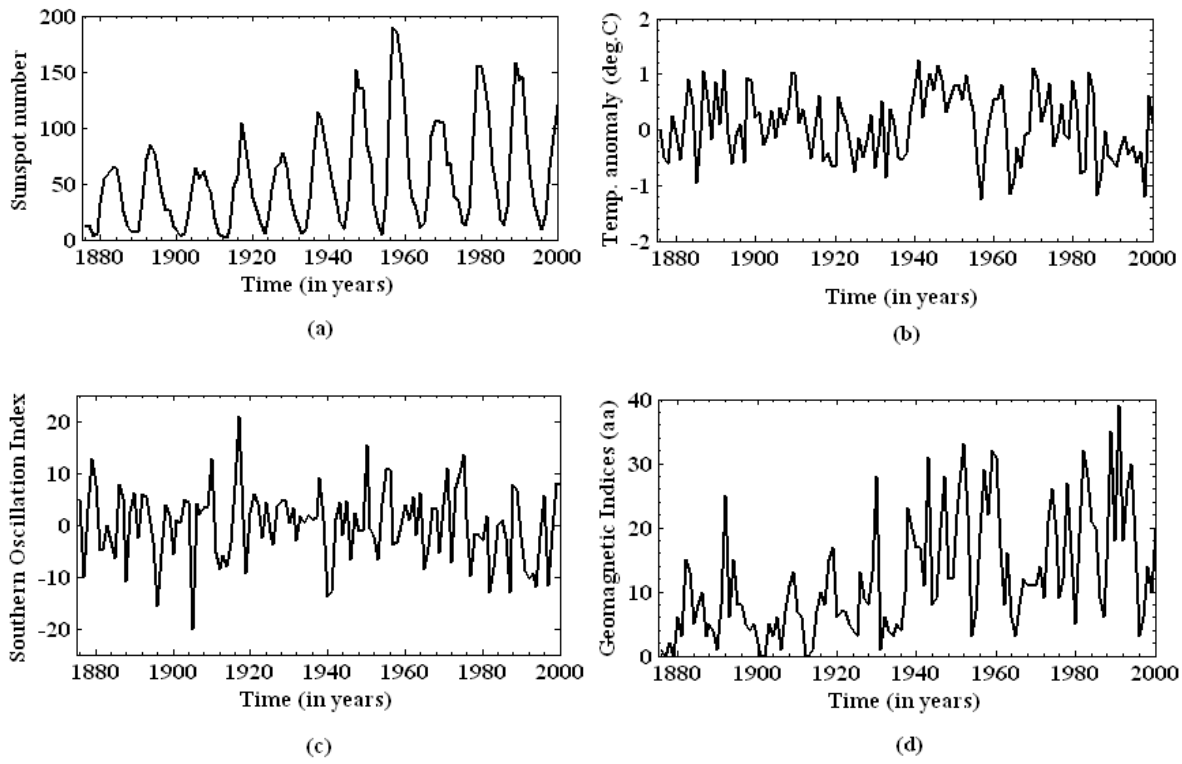

Figure 1. Time series data of (a) Sunspot Index (b) the mean pre-monsoon temperature anomalies of the Western Himalayas (Yadav et. al., 2004) (c) Southern Oscillation Index (SOI) and (d) Geomagnetic Indices (aa indices) for common period 1876-2000.

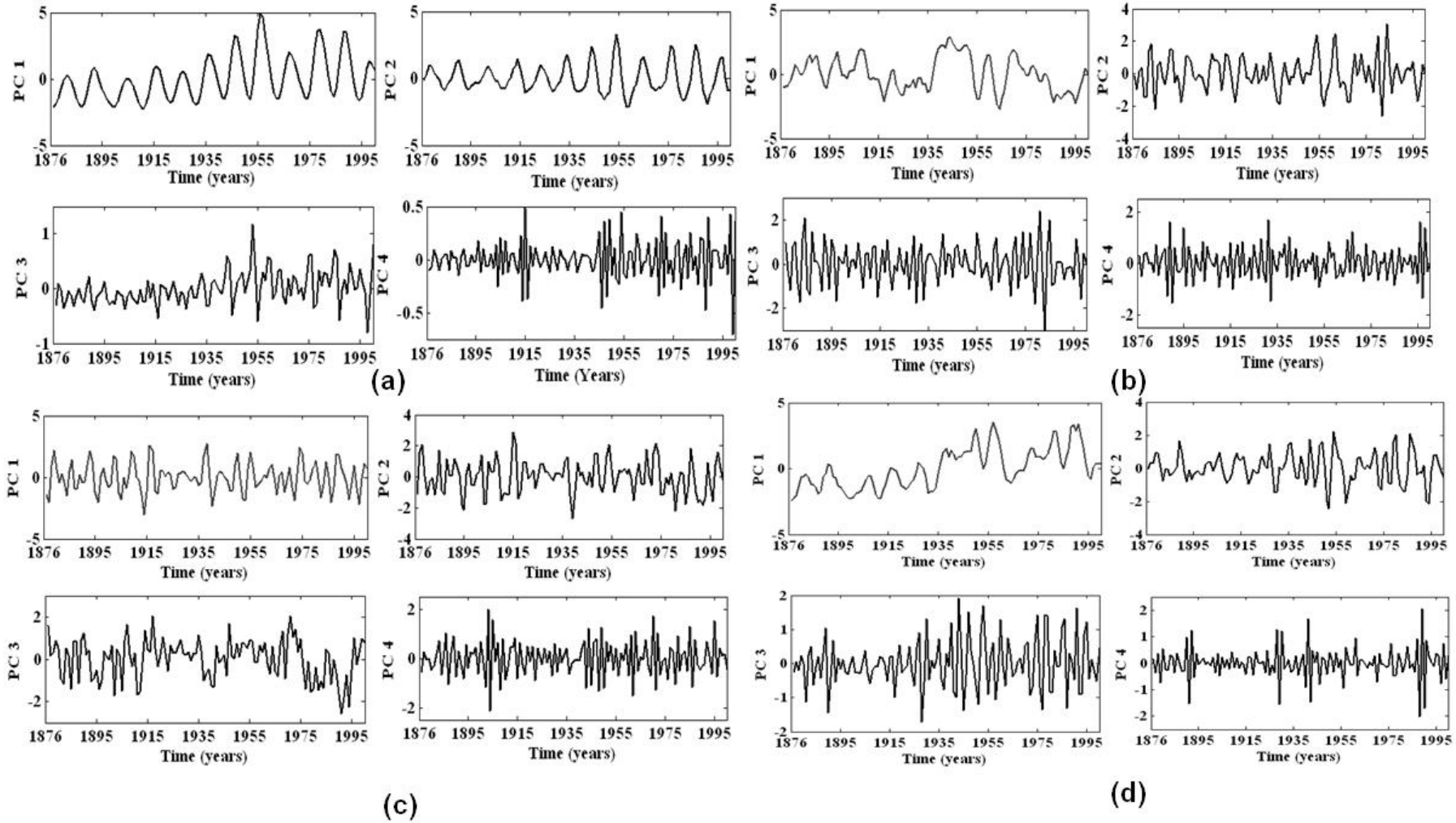

629
630 **Figure 2. First four principal components (PCs:1-4) for time series (a) Sunspot numbers (b) the mean pre-monsoon temperature anomalies**
631 **of the Western Himalayas (c) SOI index and (d) Geomagnetic Indices (aa indices) for the period 1876-2000.**

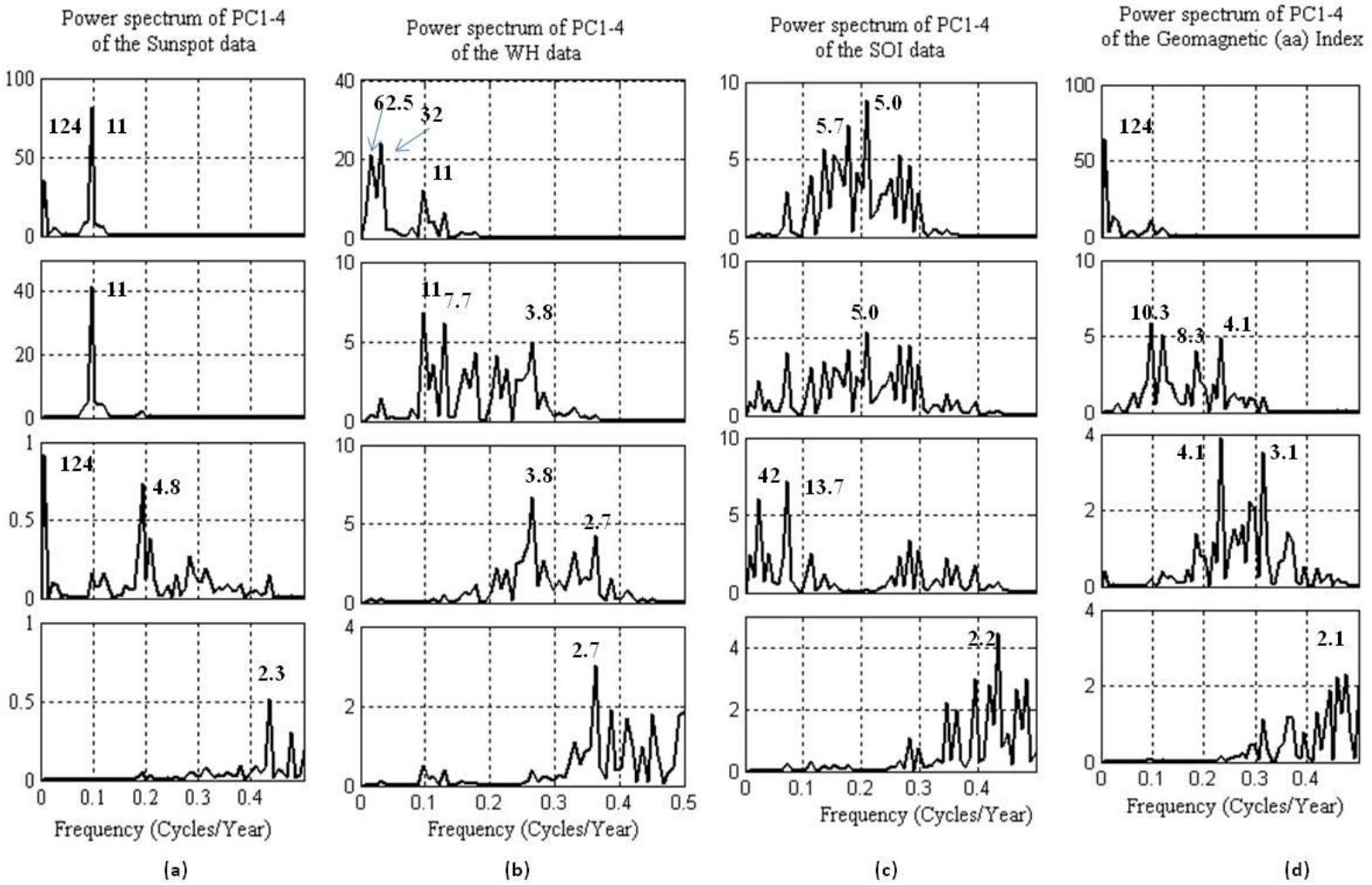

632

633 **Figure 3. Power spectra of the first four principal component (PCs) (PC1-4 shown in Fig. 2) for all the data sets with their significant**
634 **periodicities at 124, 11, 4 and 2.8 years are indicated in bold letters.**

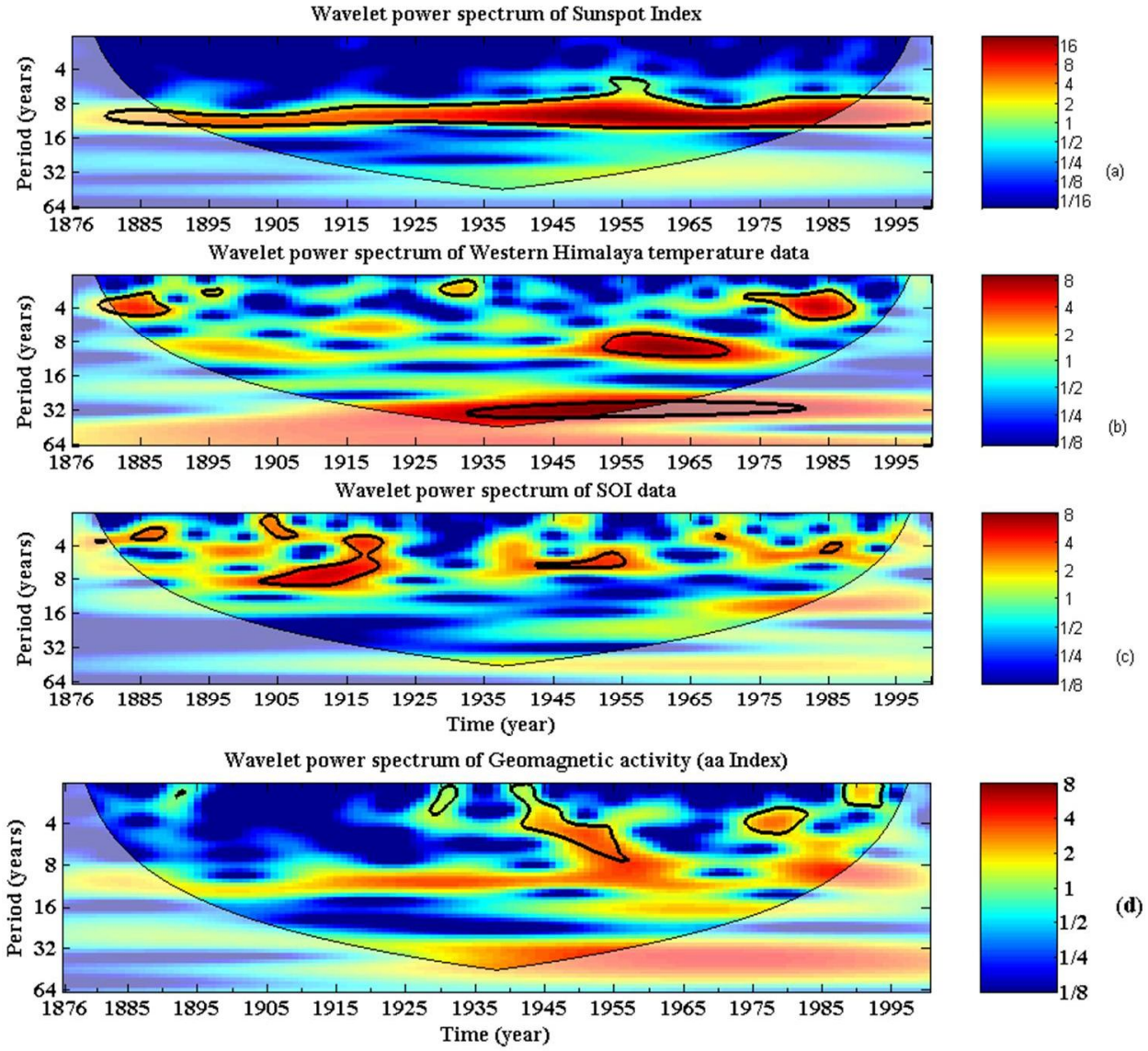

635

636 **Figure 4. Wavelet power spectrum of (a) Sunspot Number (b) Western Himalaya temperature**
637 **data (c) Southern Oscillation Index (SOI) and (d) Geomagnetic activity (aa Indices) with cone**
638 **of influence (lighter shade smooth curve) and black lines indicate significant power on 95%**
639 **level compared to red noise based on first order auto-regressive (AR(1)) coefficient. The**
640 **legend on right indicates the cross-wavelet power.**

641

642

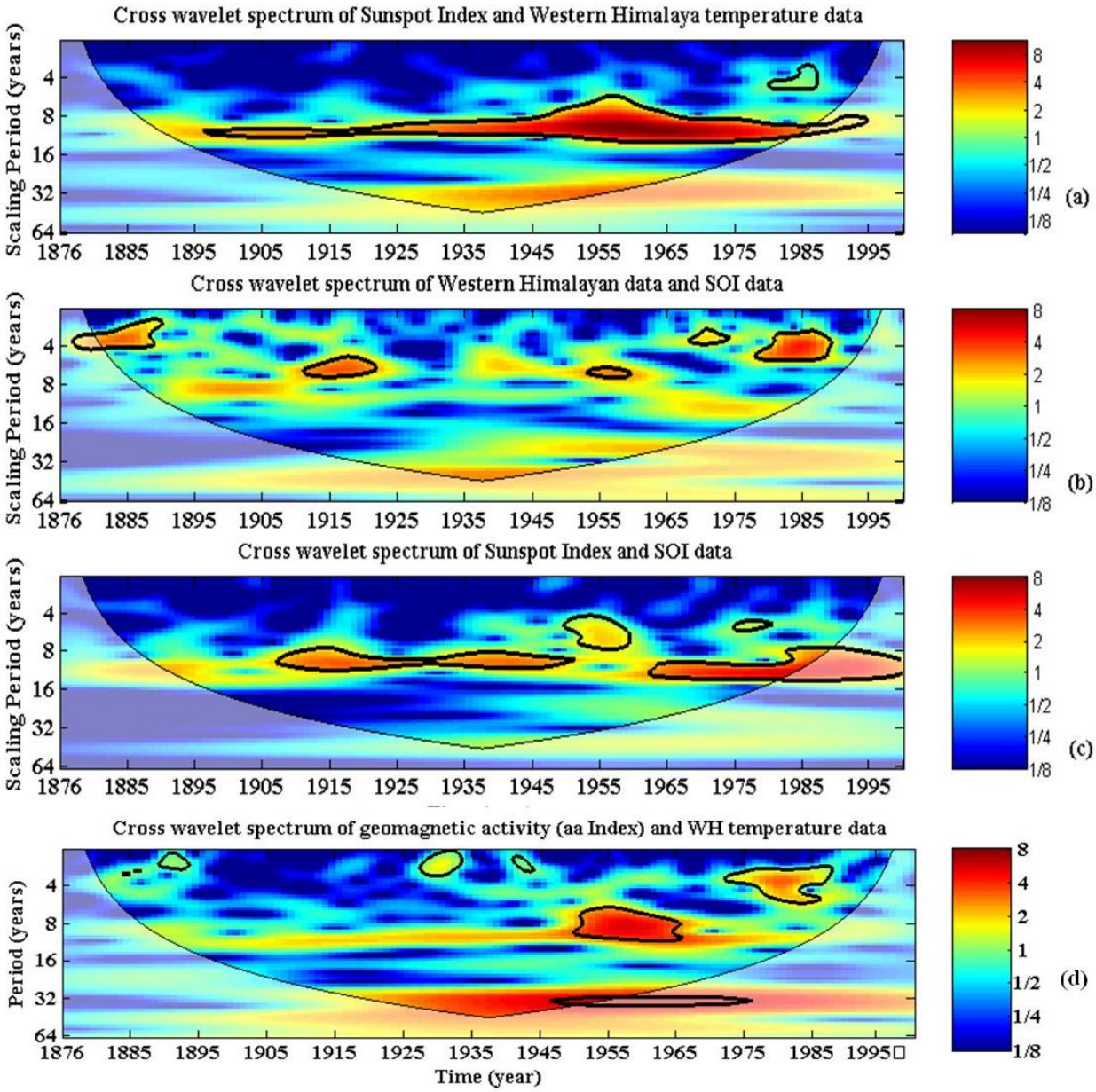

643

644 **Figure 5. Cross Wavelet spectrum between (a) Sunspot number-Western Himalayan data**
645 **(b) Western Himalayan-Southern Oscillation Index (c) Sunspot number- Southern**
646 **Oscillation Index and (d) Geomagnetic: aa indices-Western Himalayan data with cone of**
647 **influence (lighter shade smooth curve) and black lines indicate significant power on 95%**
648 **level compared to red noise based on AR(1) coefficient. The legend on right indicates the**
649 **cross-wavelet power.**

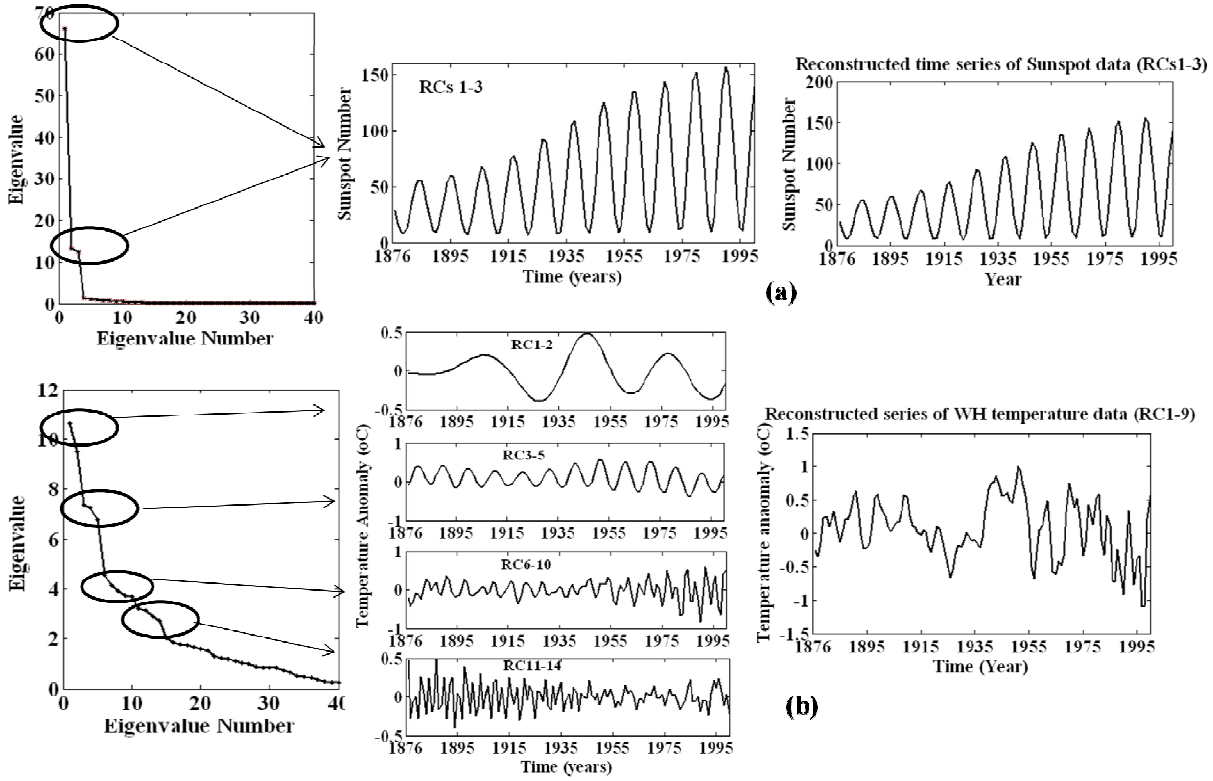

Figure 6. Singular spectra with its SSA decomposed components & its reconstructed time series for (a) Sunspot Number and (b) Western Himalaya temperature data.

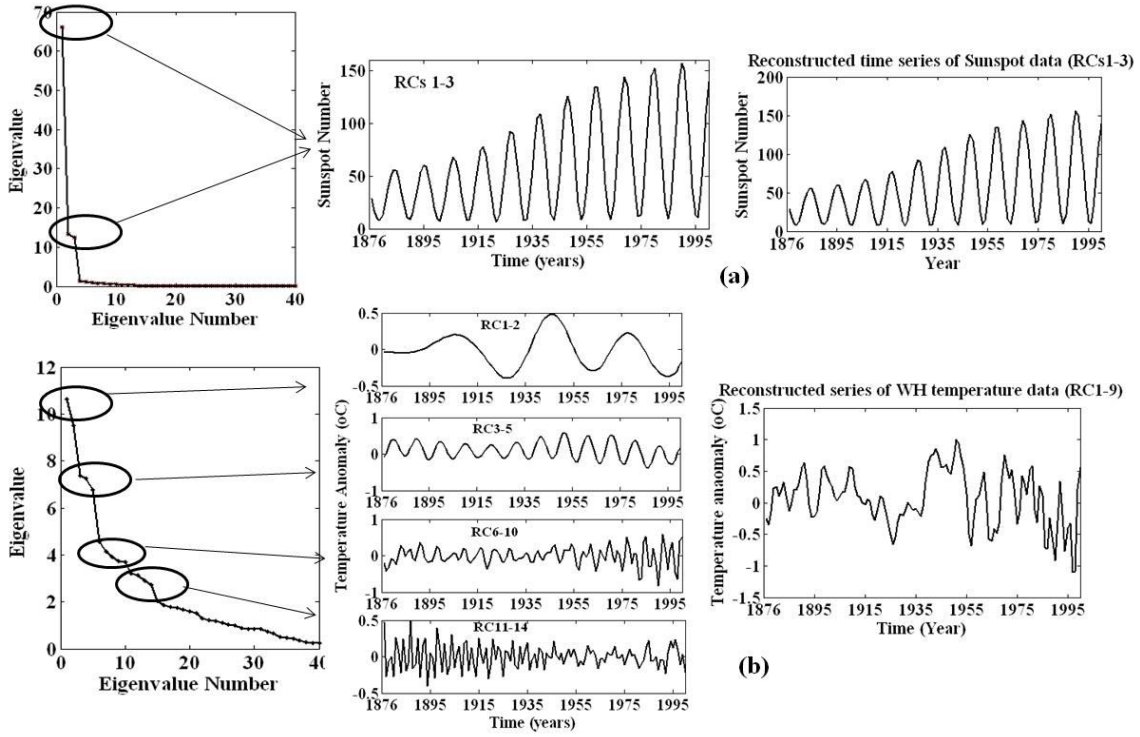

Figure 7. Singular spectra with its SSA decomposed components & its reconstructed time series for (c) SOI and (d) Geomagnetic activity (aa Indices).

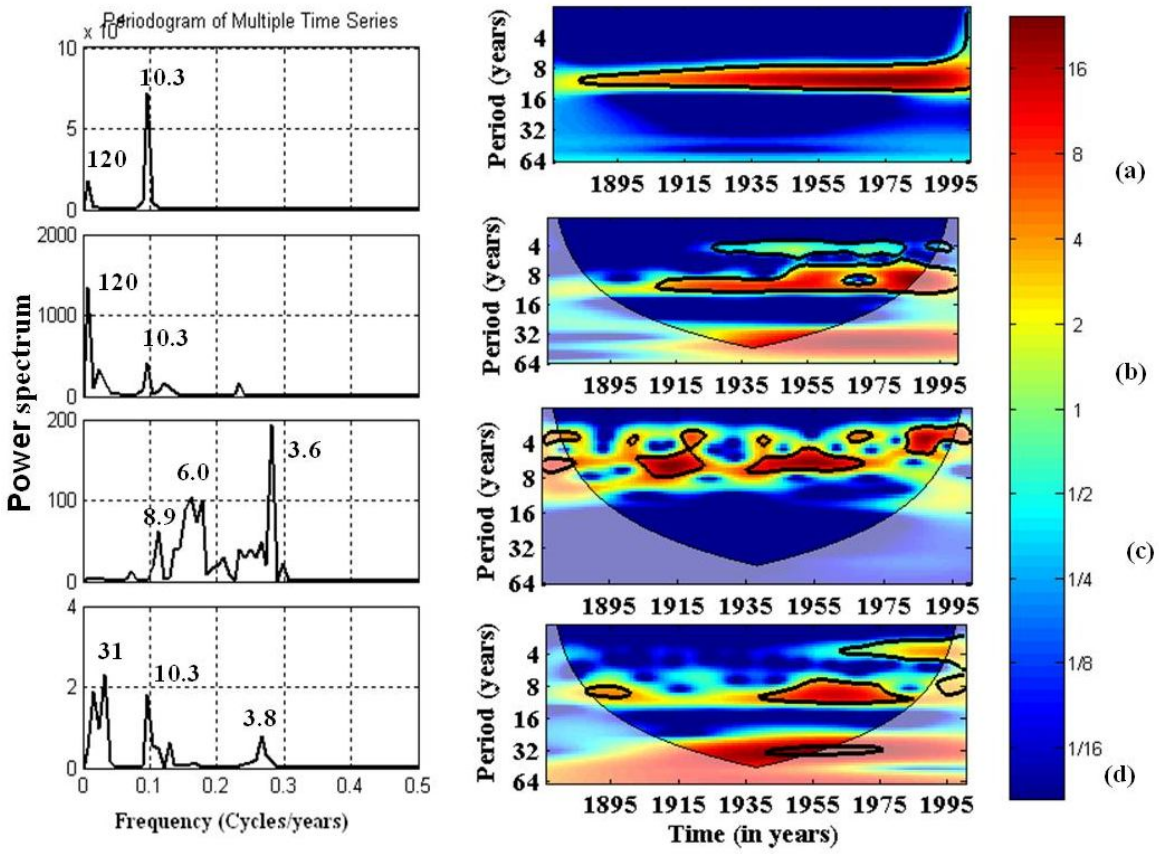

Figure 8. Power spectrum and Wavelet power spectrum of SSA reconstructed (a) Sunspot data (b) Geomagnetic Indices (aa index) (c) SOI index and (d) the Western Himalayas temperature data with cone of influence (lighter shade smooth curve) and black lines indicate significant power on 95% level compared to red noise based on AR(1) coefficient. The legend on right indicates the cross-wavelet power.

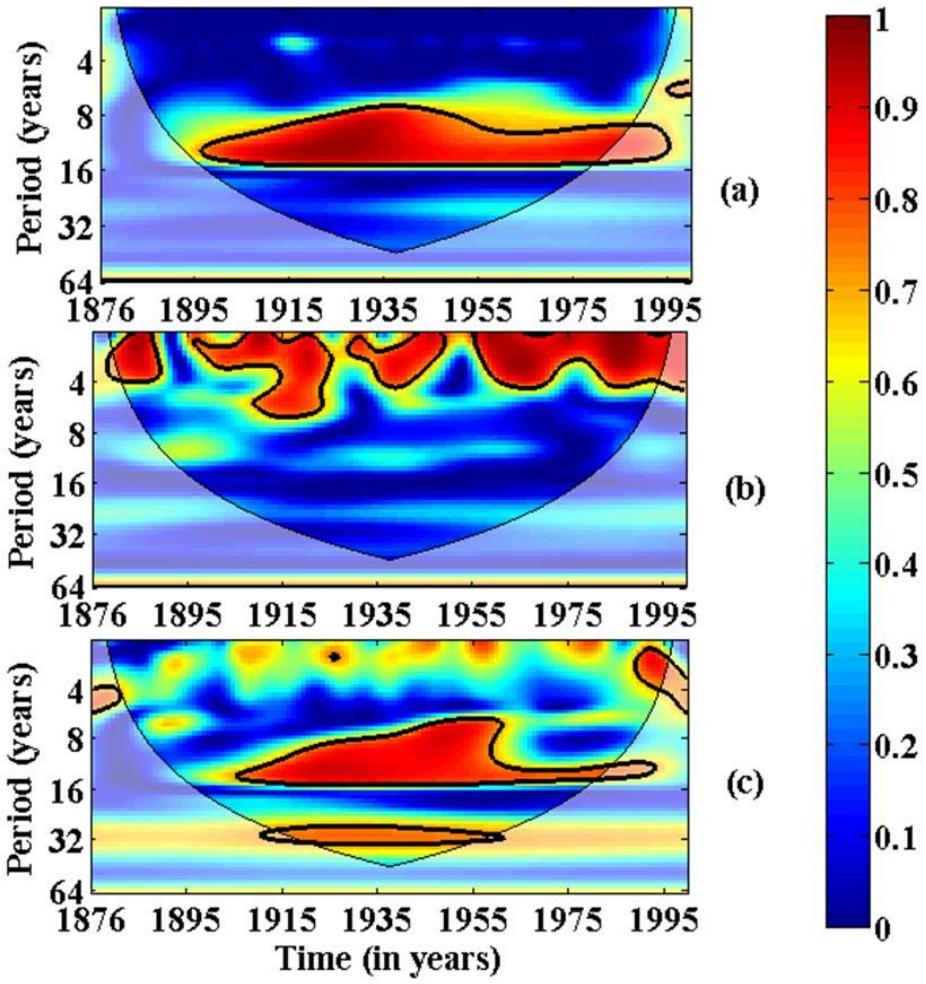

Figure 9. Squared wavelet coherence plotted for the SSA reconstructed time series between (a) WH-SSN (b) WH-SOI and (c) WH-aa index with cone of influence (lighter shade smooth curve) and black lines indicate significant power on 95% level compared to red noise based on AR(1) coefficient.

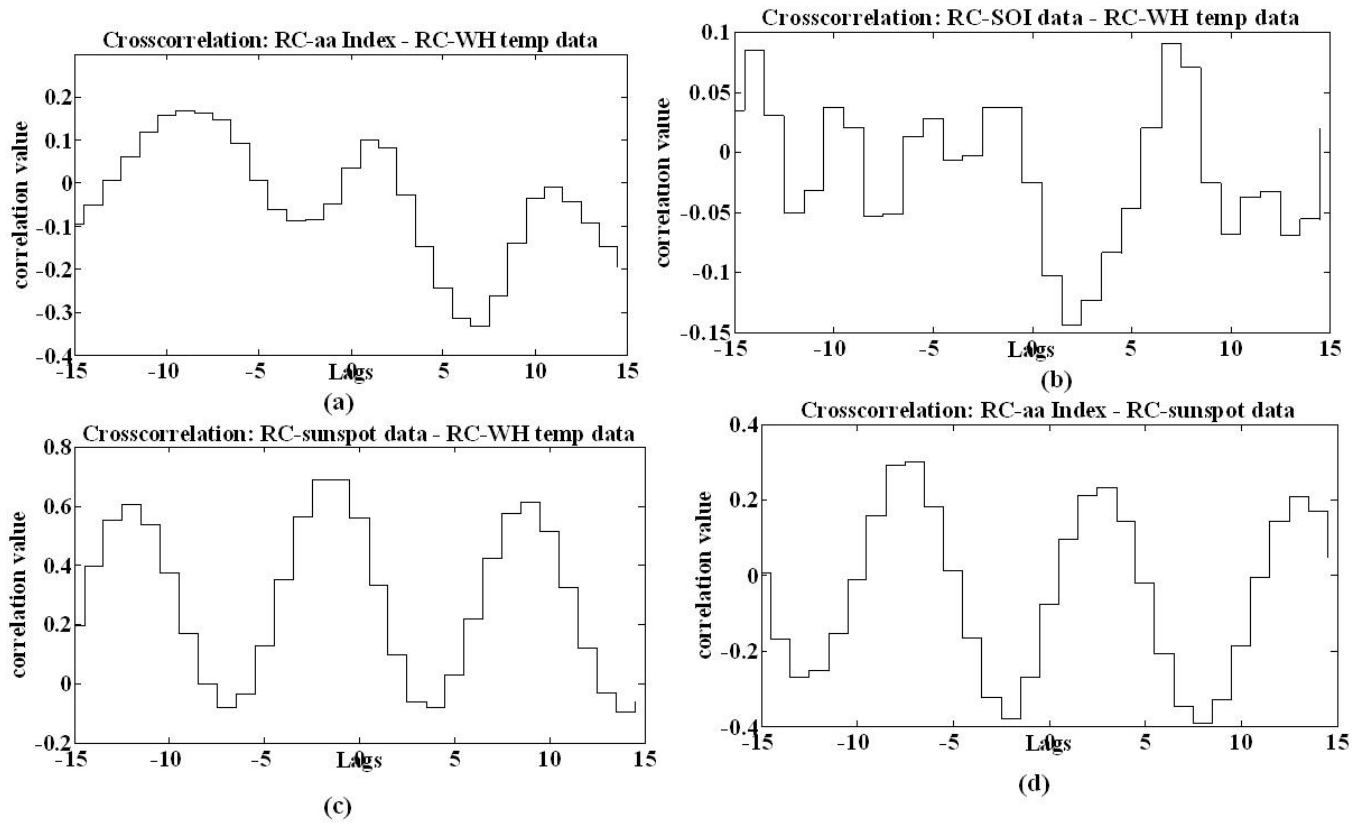

678

679 **Figure 10. Cross-correlation of SSA reconstructed time series of (a) aa Index-Western**
680 **Himalayan (WH) temperature data; (b) SOI-WH temperature data; (c) sunspot –WH data and**
681 **(d) aa Index-sunspot data.**

682

683

684